Advanced Fiber Materials (2023) 5:497–513
https://doi.org/10.1007/s42765-022-00231-x

RESEARCH ARTICLE

Processing Nomex Nanofibers by Ionic Solution Blow-Spinning for Efficient High-Temperature Exhausts Treatment

Zekun Cheng[1] · Haiyang Wang[1] · Ziwei Li[1] · Chong Yang[1] · Baopu Zhang[1] · Yiqian Zhou[1] · Yuxuan Wang[1] · Chao Jia[3] · Lei Li[2] · Hui Wu[1]

Received: 18 August 2022 / Accepted: 26 October 2022 / Published online: 8 December 2022

Abstract

Hard-to-dissolve polymers provide next-generation alternatives for high-performance filter materials owing to their intrinsically high chemical stability, superior mechanical performance, and excellent high-temperature resistance. However, the mass production of hard-to-dissolve nanofibers still remains a critical challenge. A simple, scalable, and low-cost ionic solution blow-spinning method has herein been provided for the large-scale preparation of hard-to-dissolve Nomex polymeric nanofibers with an average diameter of nearly 100 nm. After rapidly dissolving Nomex microfibers in the lithium chloride/dimethylacetamide (LiCl/DMAc) solution system, the conductive solution can be stably and conductivity-independently processed into nanofibers. The method optimizes electrospinning and avoids spinnability degradation and potential safety hazards caused by high electrical conductivity. Owing to nanofibrous structure and high dipole moment, Nomex nanofibrous filters show a stable high filtration efficiency of 99.92% for $PM_{0.3}$ with a low areal density of 4.6 g m^{-2}, as well as a low-pressure drop of 189.47 Pa. Moreover, the flame-retardant filter can work at 250 °C and 280 °C for a long and short time without shrinking or burning, respectively, exhibiting a high filtration efficiency of 99.50% for $PM_{0.3-10.0}$. The outstanding properties and low cost enable the efficient capture of PM from various high-temperature exhausts, making Nomex nanofibrous membrane an even more ideal industrial-grade air filter than polypropylene, polytetrafluoroethylene, polyimide, and ceramic nanofibrous filters.

Keywords Nomex nanofibers · Solution blow-spinning · High-temperature filtration · Flame-retardant

Introduction

Most hard-to-dissolve polymetric nanofibers enjoy the luxury of being attractive nanomaterials with inherent high-temperature resistance, corrosion resistance, excellent flame retardancy, and superior mechanical properties due to their rigid and stable molecule structures [1–4]. Although the production of hard-to-dissolve polymers is booming, the preparation of hard-to-dissolve nanofibers has been a stumbling block due to their limited solubility in common solvents, mainly restricted by numerous intermolecular and intramolecular hydrogen bonds. For example, poly(*m*-phenylene isophthalamide) (PMIA), commonly known as Nomex or meta-aramid, comprises a benzene ring and an amide group. The amide group is connected to the amide group meta-position on the benzene ring, where the amide groups on different backbones are connected by hydrogen bonds [5]. Although the intractable structure limits dissolution in common solvents, it endows Nomex with a high melting

✉ Chao Jia
jiachao0806@dhu.edu.cn

✉ Lei Li
flytolilei@126.com

✉ Hui Wu
huiwu@tsinghua.edu.cn

[1] State Key Laboratory of New Ceramics and Fine Processing, School of Materials Science and Engineering, Tsinghua University, Beijing 100084, China

[2] National Engineering Research Center of Electric Vehicles, Beijing Institute of Technology, Beijing 100081, China

[3] State Key Laboratory for Modification of Chemical Fibers and Polymer Materials, College of Materials Science and Engineering, Donghua University, Shanghai 201620, China

point and glass transition temperature, low combustion heat release rate, excellent flame retardancy, stable chemical properties, and agreeable mechanical properties [6]. Therefore, hard-to-dissolve nanofibers have a broad potential for a wide range of areas, such as high-temperature thermal insulation, modern textile, electronic material, and others [7–9].

High-temperature exhausts, mainly related to industrial fuel gas, coal furnace combustion, and automobile exhausts, seriously affect environmental governance and public health. The temperature of industrial exhausts is usually between 70 and 250 °C. For instance, the temperature of the exhausts from gas boilers, coal furnaces, glass factories, coke ovens, and fuel vehicles is typically 150–200 °C, 70–180 °C, 140–200 °C, 190 °C, and 70 °C, respectively [10, 11]. On the other hand, most high-temperature exhausts contain several acid-corrosive gases, such as H_2S, HCl, and Cl_2 [12]; and more than 70% of dust is combustible, which is easily ignited by fire or electrostatic discharge, causing dangerous explosions [13]. Particulate matter (PM) with a diameter less than 0.3 μm ($PM_{0.3}$) is considered the most hazardous contaminant [14]. As is well known, $PM_{0.3}$ can penetrate the bronchi and lungs and enter the extrapulmonary organs and central nervous system through the blood, thus posing a severe threat to human health [15, 16]. Globally, up to 91% of the population lives in an environment where air pollution exceeds World Health Organization (WHO) guidelines, and 6.7 million people die yearly from air pollution [17]. Air pollution can even contribute to the spread of global epidemics, as PMs can be transmission carriers for viruses such as COVID-19 [18, 19]. Improving filtration technology is crucial to alleviating air pollution [20]. Many strategies have been adopted to deal with the $PM_{0.3}$ emitted by high-temperature exhausts, such as sedimentation tanks, cyclone separators, electrostatic precipitators, and filtration technologies [21].

Filtration technologies are considered to be the most economical technical route as they do not require the introduction of additional energy or a complex post-treatment [22]. However, traditional commercial fibrous filters have an average fiber diameter of 1–10 μm and an average pore size of 3–20 μm, making it extremely difficult to capture $PM_{0.3}$ efficiently while maintaining a low air resistance [10]. In recent years, many studies have shown that reducing the fiber diameter effectively improves filtration performance [23]. When the fiber diameter is lowered to the range between a few tens and hundreds of nanometers, the PM capture capacity of fibrous filters is considerably improved without significantly increasing the air resistance [24, 25]. Many methods have reported excellent filtration performances of nanofibrous membranes for $PM_{0.3}$, such as the preparation of hierarchical dual-nanonet fibrous membranes based on solution blow-spinning (SBS) and self-assembly strategies [26], the preparation of high-performance nanofibrous network filters inspired by biological hybridization based on the combination of novel blend electrospinning/netting method and self-polymerization method [27], the preparation of polysulfonamide/polyacrylonitrile (PSA/PAN) composite nanofibrous filters based on electrospinning method [28], the preparation of ZnO nanowires@poly(vinylidene fluoride) (PVDF) nanofibrous membrane inspired by the grass growth based on hydrothermal method and chemical vapor deposition (CVD) [29]. Thus, nanofibrous filters are promising candidates for superior filtration materials [30, 31]. For filters of different materials, metallic filter materials can be easily oxidized and corroded in high-temperature and corrosive gas environments [32], which limits their practical applications. Ceramic fibrous filters have attracted considerable attention for high-temperature filters due to their chemical stability and high-temperature resistance [33]. However, expensive, fragile ceramic fibrous filters often cause additional debris. As for polymers, the vast majority of polymer nanofibrous filters have a working temperature lower than 200 °C [10], not meeting the requirement of high-temperature filtration. Coupled with excellent chemical and physics stabilization, hard-to-dissolve polymetric nanofibers are up-and-coming candidates for use in high-temperature industrial filters, working in harsh environments of high temperature, combustible dust, acid, and corrosiveness with low cost [34].

Finding a universal method for dissolving hard-to-dissolve polymers is essential for preparing high-performance nanofibrous membranes. Using "naked anions" as nucleophilic bases to disrupt intermolecular and intramolecular hydrogen bonds is considered an effective strategy for dissolving hard-to-dissolve polymers [35]. Many studies have shown that the LiCl/DMAc system can generate large amounts of "naked anions," which break down intramolecular and intermolecular hydrogen bonds [35–37], and is successfully used to prepare polybenzimidazole (PBI), polyimide (PI), silk, cellulose, and chitin solution [38–41]. However, for the LiCl/DMAc system, the commonly used electrospinning method is not the preferred technology because high electrical conductivity will deteriorate the spinnability and bring safety concerns. Ionic SBS is a facile, safe and straightforward preparation method, owing to the airflow driving force [42, 43]. In our study, the low-cost Nomex nanofibrous filter from the ionic SBS method with an areal density of only 4.618 g m^{-2} exhibits a high filtration efficiency (99.92%) and a low-pressure drop (189.47 Pa) for $PM_{0.3}$ at an airflow velocity of 5.33 cm s^{-1}. Moreover, at 250 °C, the Nomex nanofibrous filter with an areal density of 4.631 g m^{-2} retains a high filtration efficiency (> 99.5%) for $PM_{0.3-10.0}$. Furthermore, the other hard-to-dissolve fibrous precursor solution including PI, PBI, silk, cellulose, and chitin has been successfully prepared. It provides great potential in preparing nanofibers on a large scale via the ionic SBS method.

Experimental Section

Materials and Chemicals

Commercial Nomex microfibers were purchased from Yantai Tayho Advanced materials Co., Ltd (China). Silkworm cocoons were picked from mulberry trees beside Gongshanjian in Hangzhou, Zhejiang province (China). Chitin (1398–61–4, Industrial pure grade) was purchased from Tianjin Xiensi Biochemical Technology Co., Ltd. PI (Thermoplastic 5218, 99.9% purity) was purchased from BASF SE (Germany). PBI (99.95% purity, Mw ≈ 51,000) was purchased from Danish Power Systems (Danmark). Cotton pulp (M30, DP = 500) was purchased from Beijing North Century Cellulose Technology Development Co., Ltd. (China). LiCl (99% purity) was purchased from Meryer Chemical Technology Co., Ltd. (China). DMAc (99.9% purity) was purchased from Rhawn Chemical Reagent Co., Ltd. Polyethylene oxide (PEO, Mv ≈ 1,000,000) was purchased from Xi Ya Reagent Co., Ltd. (China). The commercial polypropylene (PP) fibrous filters and glass fibrous filters used for comparison were purchased from Hollingsworth & Vose (USA). In addition, the commercial PTFE fibrous filters were purchased from Jiangsu Xiankai (China). Commercial ceramic nanofibrous filters were purchased from Xianning Youwei Technology Co., Ltd. (China).

Preparation of Nomex Nanofibrous Membranes

The Nomex solution was prepared by dissolving commercial Nomex microfibers (1.5 g) and a small amount of LiCl (0.6 g) in DMAc (18.5 g) while magnetically stirring the mixture at 90 °C for 2.3 h**.** Subsequently, a small amount of PEO (0.035 g) was added to the Nomex solution. The mixed solution was stirred at 90 °C for about 0.2 h to obtain a well-mixed precursor solution. The solution was prepared in a glove box to prevent absorption of moisture. The configuration process of other precursor solution such as silk, PI, chitin, and cotton was shown in Supplementary Information. The Nomex nanofibrous membranes were prepared using a custom-built SBS system. In a typical procedure, the precursor solution was drawn into a 20–mL plastic syringe and extruded into a needle tip with a 0.2–mm inner diameter using a syringe pump at a fluid rate of 1.5 mL h^{-1}. The pressure of the compressed air was set to 80 kPa, and the distance between the tip and the roller collector was fixed at 30 cm. The roller collector was continuously reciprocated left and right to obtain a uniform Nomex nanofibrous membrane. The drum collector rotated at 200 rpm at a reciprocating speed of 1 cm s^{-1}. The blow-spinning process was assisted in a heated environment. A heating platform (20 cm × 20 cm in size) was kept 5 cm away from the needle tip, and an infrared heating lamp with a power of 150 W was located 20 cm away from the needle tip. Finally, the prepared uniform Nomex nanofibrous membrane was removed from the roller collector and heated in an oven at a temperature of 60 °C for 1 h.

Characterization

A field-emission scanning electron microscope (Zeiss, Germany) was used to observe the morphology of the samples, and an energy-dispersive spectrometer (EDS) detector (Zeiss, Germany) was used to determine the elemental composition. The distribution of the fiber diameters was obtained by measuring the diameter of more than 100 fibers in the scanning electron microscope (SEM) images using the Image-Pro Plus software (Media Cybernetics, USA). The pore diameter and porosity of a typical Nomex nanofibrous membrane with an areal density of 4.251 g m^{-2} at room temperature (25 °C) and high temperature (200 °C) were measured using an automatic mercury porosimeter (MicroActive AutoPore V 9600 2.03.00, Micromeritics Inst Inc., USA). The conductivity of the Nomex precursor solution was measured by conductivity benchtop meters (VSTAR20 series, ThermoFisher Scientific, USA). An X-ray diffractometer (XRD, D/max-2500/PC, Rigaku, Japan) with a Cu Kα radiation source was used to obtain the XRD patterns of the samples in the 2θ range of 10°–60° at a scanning rate of 10°min^{-1}. The blow-spinning process was observed using a high-speed camera (Os7, IDT Vision, USA) equipped with an F-mount lens (atx-i 100 mm F2.8 FF MACRO, Tokina, Japan). All high-speed images were captured at a frame rate of 8,000 fps with an exposure time of 60 μs and eventually played back at a frame rate of 24 fps. Other characterization can be seen in Tests S1 and S2.

Dipole Moment Calculation

Density functional theory (DFT) calculations were performed using the Gaussian 09 software package [44]. The repeating units of the Nomex, polytetrafluoroethylene (PTFE), PAN, and PP filters were fully optimized at the B3LYP/6–311+G (d, p) level without an imaginary frequency.

Room Temperature Filtration Test

The filtration efficiency and pressure drop at room temperature were measured using an automatic filtration tester (8130A, TSI, USA). A 2% sodium chloride (NaCl) solution was used to generate a NaCl aerosol with a mass median diameter of 0.26 μm and a median count diameter of 0.075 μm. Unless otherwise specified, the filtration efficiency and pressure drop in this work were measured at a

continuous airflow rate of 32 L min^{-1} (5.33 m s^{-1}). All filter performance test results were obtained by averaging three sets of data. The quality factor *(QF)* was derived according to the following equation:

$$QF = [-ln(1-\eta)]/\Delta P, \quad (1)$$

where ΔP is the pressure drop before and after the airflow through the membrane, η is the efficiency of capturing PMs.

High-Temperature Filtration Test

A high-temperature filtration test device has been customized. Firstly, two quartz glass tubes 500 mm in length and 42 mm in inner diameter have been designed and Nomex nanofibrous membrane between the two quartz glass tubes has been placed. Subsequently, the quartz glass tubes were placed in a temperature-adjustable tube furnace (OTF-1200X, HF-Kejing, China). Two ends of the quartz glass tubes were connected with the air inlet pipe, the air outlet airflow was generated by an air compressor (1500X4, OTS, China), and PM was produced by burning incense. The inflow of the compressed air flow along the intake pipe was controlled by a flow meter, causing PM to enter the quartz glass pipe. Two PM particle counters (DT-9880 M, CEM, China) were connected to the inlet and outlet of the quartz glass tube to measure the number of PM particles of different sizes. The PM particle counters comprised six channels, which could detect the number of PM particles with diameters of 0.3, 0.5, 1.0, 2.5, 5.0, and 10.0 μm. The accumulation mode of the particle counters has been used in measuring the $PM_{0.3-10}$ value with an acquisition time of 30 s. Finally, the high-temperature filtration efficiency of the Nomex nanofibrous membrane was calculated by taking the difference between the number of PM particles with a given size before and after filtration. The cumulative mode of the PM particle counters has been used in measuring the $PM_{0.3-10}$ value at the exhaust port when the vehicle engine speed was 3,000 rpm. The test duration was 30 s. By denoting the particle number of each channel obtained before and after installing the Nomex nanofibrous membrane filter as C_1 and C_2, respectively, η can be calculated as follows:

$$\eta = 1 - \frac{C_1}{C_2}. \quad (2)$$

In the high-temperature filtration stability test, the Nomex nanofibrous membrane was continuously heated in a muffle furnace at 250 °C for 15 consecutive days and tested their filtration performance daily using a TSI 8130A filtration tester. All filter performance test results were obtained by averaging three sets of data.

Results and Discussion

Preparation of Nomex Nanofibrous Membranes

A DMAc solution system containing anhydrous LiCl was used to dissolve Nomex microfibers (Fig. 1a). After electromagnetic stirring in LiCl/DMAc solution system at 90 °C for 2.5 h, Nomex microfibers were completely dissolved and a translucent precursor solution was successfully prepared (Fig. 1b). The anhydrous LiCl in DMAc can break the hydrogen bonds between the Nomex molecular chains through complexation, which resulted in the dissolution of the commercial Nomex microfibers into the solvent. In this system, Li^+ and DMAc form an ion–dipole complex: $[DMAc + Li]^+$. Due to the polar aprotic property of DMAc and the inability of hydrogen atoms in DMAc to form hydrogen bonds, Cl^- cannot be solvated [45]. Therefore, Cl^- will have greater freedom to break the intermolecular and intramolecular hydrogen bonds in hard-to-dissolve polymers (Fig. 1c) [37]. In addition, a small amount of PEO was added to increase the spinnability of the precursor solution. Based on the same mechanism, PBI, silk, cellulose, chitin, and PI polymer have been dissolved successfully by the LiCl/DMAc system, all of which are expected to be converted into nanofibers (Fig. 1d).

Through the ionic SBS method, hard-to-dissolve nanofibers can be prepared stably to uniform nanofibers driven by the high-speed airflow on a large scale in the whole dissolvable range in LiCl/DMAc system (Fig. S1). However, the key to electrospinning is the accumulation of free charges at the solution interface and liquid stretching induced by the tangential electric field. Thus, the Nomex nanofibrous membrane cannot be easily prepared by electrospinning when the solution conductivity is relatively high. Moreover, the generation of electric sparks during electrospinning introduces potential safety hazards. Specifically, when the mass fraction of LiCl is 2% (Fig. 1e: Region 1), the solution has relatively high conductivity (4.35 mS cm^{-1}) with an excessively long dissolution time. When the mass fraction of LiCl is 3–5% (Fig. 1e: Region 2), the solution conductivity is 5.62–5.72 mS cm^{-1} with a higher dissolution rate. However, the relatively high conductivity makes the solution difficult to form stable Taylor cones, and thus Nomex nanofibrous membrane cannot be prepared readily. When the mass fraction of LiCl is 5–10%, the conductivity of the solution decreases. Although Nomex fibers can be prepared in this region, many fibers are bundled together to

form micron-sized fibrous bundles due to the limited traction caused by the conductivity of the solution (Fig. 1e: Region 3 and Fig. S2) [46, 47].

In the ionic SBS process, the polymer precursor solution is drawn by the airflow, and a jet is first formed when the drawing force is greater than the surface tension (Figs. 2a and S3). Then, benefiting from heating and the strong gas–liquid interface disturbance, the solvent volatilizes rapidly to form ultra-fine nanofibers, enabling a safe, scalable, simple, and cost-effective process. Here, we readily refined Nomex microfibers (diameter ≈ 19 μm) into Nomex nanofibers (diameter ≈ 100 nm), which implies that a commercial Nomex microfiber has been successfully processed into more than 30,000 Nomex nanofibers (Fig. 2b). These Nomex filters composed of nanofibers are expected to achieve a highly efficient filtration of PM in exhausts (Fig. 2c). Moreover, solution jetting and fiber whipping were visualized through high-speed videography (Fig. 2d–f, Video S1). Under the action of high-speed airflow in the ionic solution blow-spinning process, the sheer force induced by the airflow refines the solution extruded from the needle tip, and first forming a Taylor cone, then forming a liquid jet along the flow direction, and finally whipping violently. Strong gas–liquid interface disturbance and temperature gradient field promote the volatilization of DMAc, ultimately leaving high-quality nanofibers.

A typical Nomex nanofibrous membrane with different thicknesses is presented in Fig. S4; these membranes can be widely used in automotive exhaust filters, industrial exhaust filters, masks, and other scenarios (Fig. S5). Alternatively, a breathable cage-like collector can be placed behind the drum collector, where excess nanofibers can form a porous three-dimensional nanofiber sponge. Based on multi-needle integrated spinning devices and roll-to-roll collection devices, the large-scale production of Nomex nanofibrous membranes can be easily achieved [48]. Moreover, Nomex nanofibrous sponges prepared by vacuum freeze-drying technology can be used for thermal insulation, photocatalytic, energy storage, and wound healing (Fig. S6) [49–52].

Structure and Properties of Nomex Nanofibrous Membranes

The microscopic size of the Nomex nanofibrous membrane was observed via SEM. The SEM images show that these Nomex nanofibers have uniform morphologies, smooth surface, and high aspect ratio (Fig. 3a). Through adjusting parameters, including precursor solution injection rate, polymer solution concentration, and airflow velocity, the average diameter of the Nomex fibers is consistent in the range of 100–200 nm, highlighting the reliability of the spinning process (Fig. S7). It is proved that under the action of strong gas–liquid interface disturbance and temperature gradient field, the solvent volatilizes rapidly, and the nanofibers are well formed. It is also fully demonstrated that the solution and the ionic SBS method have excellent stability, laying a good foundation for large-scale production. The fiber structure of a single Nomex nanofiber was also observed via transmission electron microscopy (TEM), and its electron diffraction pattern consists of an amorphous diffraction ring (Fig. 3b). An amorphous peak appears in the XRD pattern of a typical Nomex nanofibrous membrane, indicating that the prepared Nomex nanofibers are amorphous (Fig. S8). The Fourier-transform infrared spectroscopy (FTIR) spectrum of the precursor solution and Nomex nanofibers demonstrate their successful preparation. (Fig. S9, Fig. 3c, see Test S3 for details).

Many studies have shown that the finer the nanofiber diameter, the better the filtration performance of the nanofibrous filters [53]. To achieve an excellent filtration performance, a typical Nomex nanofibrous membrane with an average fiber diameter of 111 nm (Fig. 3d) was prepared, and the porosity of this nanofibrous membrane was around 92.36% at room temperature (Fig. 3e, Table S1). The relatively high porosity of the Nomex nanofibrous membrane can provide channels for airflow [54], thereby reducing air resistance during filtration. After heat treatment at 200 °C for 25 h, the Nomex nanofibrous membrane maintained a high porosity (86.78%) (Fig. 3e, Table S1). In addition to the potential excellent filtration performance and thermal stability, the consumption and cost are also relatively low. The raw material cost of Nomex nanofibers is 63.36 \$ kg^{-1}, which is lower than other potential high-temperature filter materials, including PI, poly(1,4-phenylene sulfide) (PPS), and PTFE powders (Fig. S10). In addition, the Nomex nanofibrous membranes have minimal consumables, capturing more than 99.9% of $PM_{0.3}$ with an areal density of only 4.618 g m^{-2}. The consumables are quantified in terms of the areal density. At the same filtration efficiency of over 99.5% for $PM_{0.3}$, the areal density of the Nomex nanofibrous membranes is considerably lower than that of PI nanofibrous membranes (6.61 g m^{-2}), polyvinyl chloride/polyurethane (PVC/PU) fibrous membranes (21 g m^{-2}), commercial PP filters (40.88 g m^{-2}), and commercial glass fibrous filters (80.54 g m^{-2}) (Fig. S11). In other words, to achieve the same level of filtration efficiency, Nomex nanofibrous membranes consume 88.7% and 94.3% less material compared to current commercial PP and glass fibrous filters, respectively.

A Nomex nanofibrous membrane with an areal density of 1.890 g m^{-2} can capture 95.42% of $PM_{0.3}$, and that of 3.780 g m^{-2} can capture 99.6% of $PM_{0.3.}$ To demonstrate the advantages of Nomex nanofibrous membranes in terms of low areal density, the filtration performance and areal density of Nomex nanofiber membranes were compared with other fibrous air filters, as shown in Fig. 3f. The performance of the Nomex nanofibrous membrane is better than most of the polymer-based fibrous filter materials,

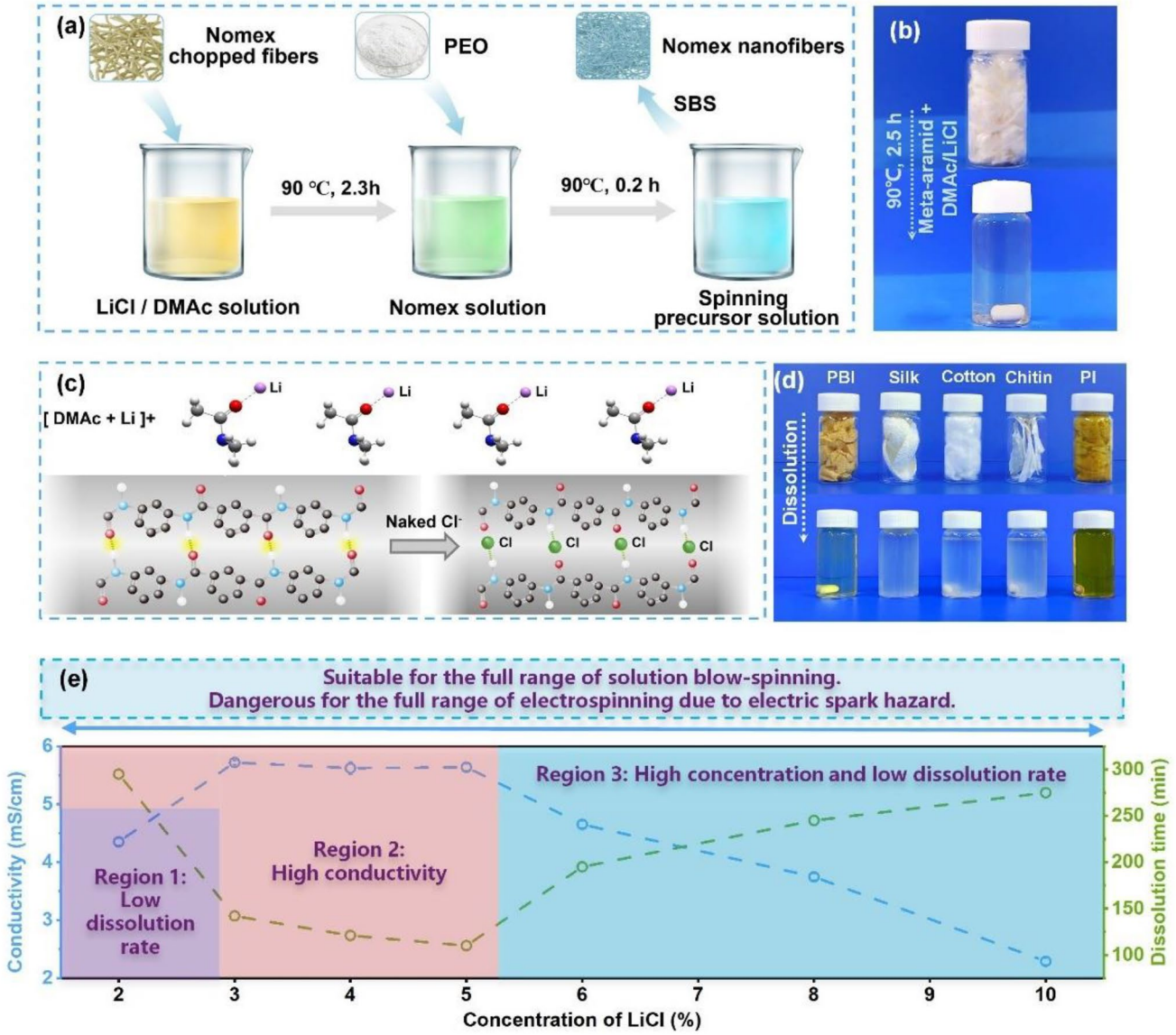

Fig. 1 Preparation of Nomex and other hard-to-dissolve nanofibrous precursor solution. **a** Schematic diagram of the preparation process of Nomex precursor solution. **b** A 20-mL bottle of successfully prepared clear Nomex precursor solution. **c** Dissolution mechanism of Nomex in LiCl/DMAc solution. **d** Different hard-to-dissolve fibrous precursor solution was successfully prepared in LiCl/DMAc system. **e** The relationship between conductivity, dissolution time, and LiCl concentration of LiCl/DMAc solution system: the electrospinning process of solution system is accompanied by a large number of electric sparks, and relatively high conductivity represents high spark risk, relatively low conductivity represents low dissolution efficiency

such as PVDF/graft (83.00%, 8 g m^{-2}) [55], PP (99.36%, 60 g m^{-2}) [56], PVC/PU (99.50%, 21 g m^{-2}) [57], PAN (98.89%, 7.49 g m^{-2}) [58], PI (99.73%, 6.61 g m^{-2}) [53], fluorinated polyurethane/PAN/PU (FPU/PAN/PU, 95.91%, 12.02 g m^{-2}) [58], polyamide6/soy protein isolate (PA6/SPI, 99.53%, 11.4 g m^{-2}) [59]. Additionally, the performance of the Nomex nanofibrous membranes is better than most of the ceramic-based fibrous filter materials, such as γ-alumina (99.85%, 9.28 g m^{-2}) [60] and TiO_2 (96.05%, 7.1 g m^{-2}) [61], and is apparently superior to that of commercial glass fibrous filters (99.89%, 80.542 g m^{-2}). After calculation, the raw material cost for preparing Nomex nanofibrous membrane is 1561.74 RMB kg^{-1}. The filtration efficiency for $PM_{0.3}$ is 99.92%, 99.60%, 98.51%, and 95.40%, and the corresponding areal densities are 4.618 g m^{-2}, 3.780 g m^{-2}, 2.865, and 1.890 g m^{-2}, respectively. Converting to area production cost, the area production cost of a Nomex nanofibrous membrane with a filtration efficiency of 99.92%, 99.60%, and 98.51% is 7.21 RMB m^{-2}, 4.47 RMB m^{-2}, and 2.95 RMB m^{-2}, respectively, which is close to the area production cost of bulk industrial commodity PP melt-blown

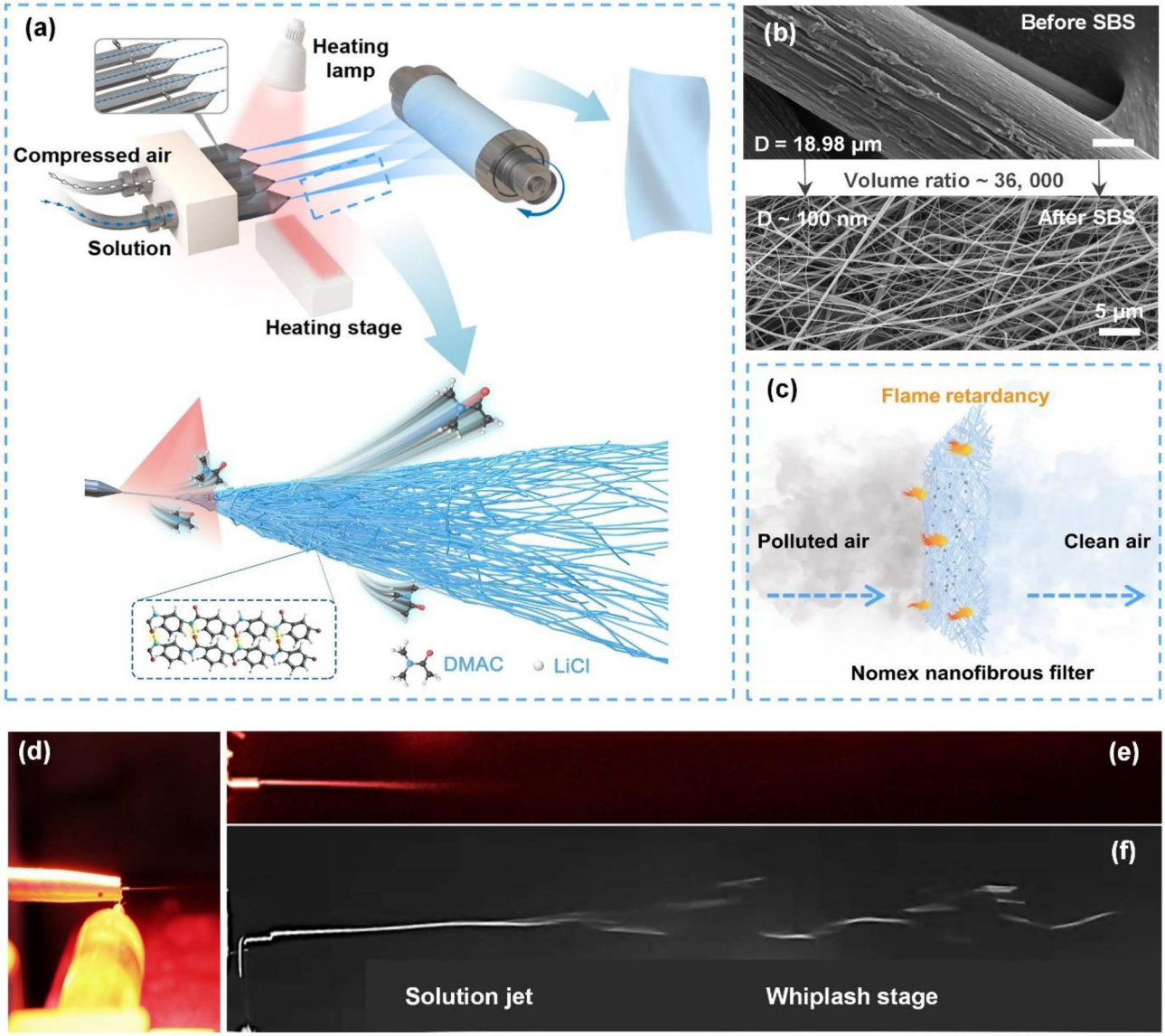

Fig. 2 Preparation of hard-to-dissolve nanofibrous membranes via ionic SBS. **a** Schematic diagram of the preparation process of blow-spinning Nomex nanofibrous membranes. **b** Commercial Nomex microfibers with an average fiber diameter of 19 μm were successfully fabricated into Nomex nanofibers with an average fiber diameter of 98 nm by ionic SBS. **c** Schematic diagram of the fire-retardant, high-temperature resistant Nomex nanofibrous filter used for high-efficiency filtration. **d** Image of spinneret nozzle part during spinning. **e** Enlarged image of spinneret nozzle part during spinning. **f** High-speed camera image of spinneret nozzle part during preparation, it could be seen that the solution forms a jet and then starts to whip

cloth and lower than that of high-temperature resistant PTFE filter.

We conducted a simple flame-burning test to evaluate the excellent flame retardancy of Nomex nanofibrous membranes. Figure 3g and Video S2 show that no delayed combustion or melting occurs when the membrane encounters the flame. Furthermore, Fig. 3g and Video S2 also demonstrate the excellent self-extinguishing properties of the Nomex nanofibrous membranes. After igniting a Nomex nanofibrous membrane with a small fire extinguisher for 5 s, the flame went out immediately when the fire extinguisher was turned off. Further, thermal gravimetric analysis (TGA) and differential thermal analysis (DTA) were conducted to investigate the thermal stability and high-temperature resistance of Nomex nanofibrous membranes (Fig. 3h). The DTA result shows that in the argon atmosphere, the Nomex nanofibrous membranes exhibit a gentle exotherm without any clear melting endothermic peaks below 700 °C during the heating process. The TGA results show that in the air atmosphere, the Nomex nanofibrous membranes only lose

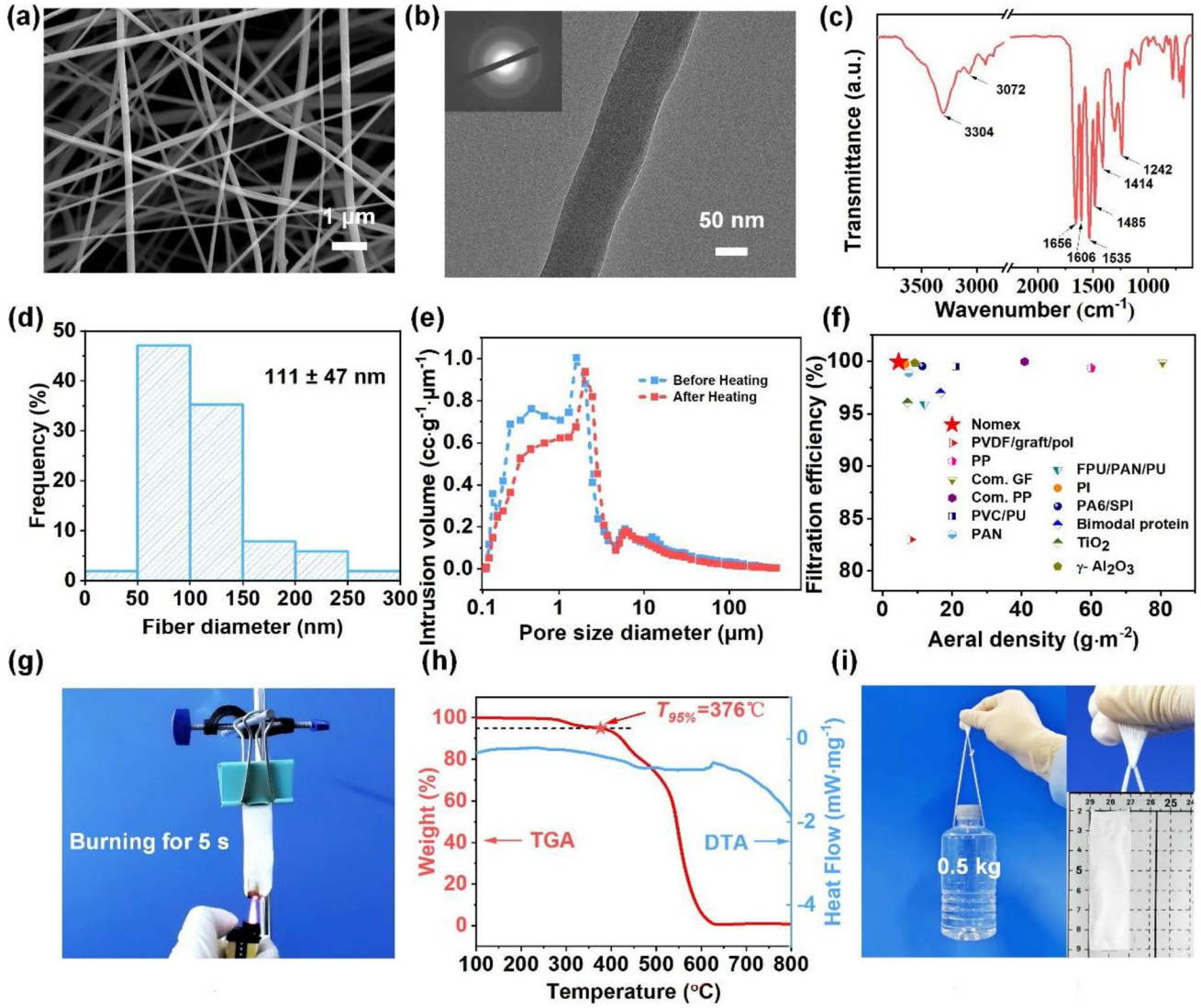

Fig. 3 Characterization of the Nomex nanofibrous membranes. **a** SEM image of a Nomex nanofibrous membrane. **b** TEM and diffraction ring images of a Nomex nanofiber. **c** FTIR spectrum of blow-spinning Nomex nanofibers. **d** Histogram showing the Nomex nanofibers' diameter distribution based on measurements of more than 100 fibers. **e** Area pore size distribution of a typical Nomex nanofiber membrane measured by an automated mercury porosimeter before and after being heated at 200 °C for 25 h. **f** Comparison of the areal density and filtration efficiency for $PM_{0.3}$ of the Nomex nanofibrous membranes with other air filter materials. **g** Image showing the flame retardancy and fire safety of the Nomex nanofibrous membrane after burning for 5 s. **h** TGA and DTA curves of the Nomex nanofibrous membrane. **i** Demonstration that a Nomex nanofibrous membrane with dimensions of 70 mm (length) × 20 mm (width) × 0.05 mm (thickness) can stably lift a 0.5-kg bottle

5% of mass at 376 °C, which is higher than that of most polymer nanofiber membranes, such as PTFE (368 °C), PAN (295 °C), and PP (221 °C) membranes (Fig. S12). According to the differential scanning calorimeter (DSC) results, the glass transition temperature (T_g) of the Nomex nanofibrous membranes is around 245 °C (Fig. S13). The above tests demonstrate the high-temperature resistance of Nomex nanofibrous membranes. The absence of molten droplets at high temperature indicates the high-temperature safety of the Nomex nanofibrous membranes.

It is essential to analyze their flame retardancy further to investigate the safety of the Nomex nanofibrous filters when used at high temperature. Generally, materials with a limiting oxygen index (LOI) greater than 27% are considered flame-retardant. The oxygen index test reveals that the LOI value of the Nomex nanofibrous membranes is 28.39% (Tables S2–S3), which proves that it is a flame-retardant material (Fig. S14). The heat release rate (HRR) is one of the most critical thermal parameters for evaluating the flame retardancy and fire safety of polymers [62]. The peak value

of the heat release rate (pHRR) of the Nomex nanofibrous membranes (27.608 W g^{-1}) was obtained by conducting a micro-scale combustion calorimetry (MCC) measurement; the obtained value is lower than that of most polymer nanofibrous membranes, such as PTFE (401.280 W g^{-1}), PAN (121.533 and 27.608 W g^{-1}), and PP (447.361 W g^{-1}) membranes. The total heat release (total HR) value of the Nomex nanofibrous membranes was calculated to be 4.9 kJ g^{-1}, which is lower than those of PTFE (19.1 kJ g^{-1}), PAN (11.6 kJ g^{-1}), and PP (341.0 kJ g^{-1}) membranes (Fig. S15). Low pHRR and total heat release (total HR) values indicate that the filter is less likely to present a fire hazard. In addition, the HRR curves of Nomex nanofibrous membranes are flatter, which suggests that Nomex nanofibrous membranes burn more slowly.

Mechanical tensile tests were performed using a universal testing machine. The test results show that the average tensile strength of the Nomex nanofibrous membranes at room temperature is 4.36 MPa, corresponding to an average elongation of 68.05% (Fig. S16). Fig. S17 shows the stress–strain curve of a typical Nomex nanofibrous membrane at room temperature. Figure S16 shows the average tensile strength and elongation of Nomex nanofibrous membranes heated at 200 °C for a different time. The test shows that the tensile strength of the membranes remains close to 80% after heating at 200 °C for 50 h. In addition, the dynamic thermodynamic analyzer (DMA) test results reveal that the Nomex nanofibrous membranes can maintain a tensile strength of more than 4 MPa while operating at a high temperature of 250 °C for 10 min (Fig. S18). The mechanical properties of the Nomex nanofibrous membrane are also displayed in Fig. 3i, indicating a typical Nomex nanofibrous of 70 mm (length) × 20 mm (width) × 0.05 mm (thickness) can stably lift a 0.5-kg bottle of water (Video S3). In addition, considering the acidity of industrial flue gas [63, 64], a Nomex nanofibrous membrane was soaked in a 3 mol L^{-1} hydrochloric acid solution for 24 h to test its acid corrosion resistance. Its surface morphology and structure via SEM and FTIR were investigated to demonstrate the stability of the membrane after being corroded in an acidic solution. The SEM image shows that the membrane retains a smooth surface morphology. All characteristic peaks in the FTIR spectrum are consistent with those shown in Fig. 3c, demonstrating the well acidic-corrosion resistance (Fig. S19).

To demonstrate the excellent filtration performance of the Nomex nanofibrous membranes, their filtration performance for different areal densities at different airflow velocities was tested. The relationship between the spinning time, areal density, filtration efficiency (η), pressure drop (ΔP), and QF is shown in Fig. S20. A higher QF value means a better filtration performance of a filter. Figure 4a shows that as the areal density of the membrane increases, the filtration efficiency gradually increases, while the rate of increase gradually decreases. For instance, at an airflow velocity of 5.33 cm s^{-1}, Nomex nanofibrous membranes with areal densities of 1.553, 1.890, 2.865, 3.780, and 4.618 g m^{-2}, exhibit $\eta = 92.24\%$, 95.42%, 98.51%, 99.60%, and 99.92%. Further, the airflow velocity has little influence on the filtration efficiency of the Nomex nanofibrous membranes, especially when the areal density is greater than 1.890 g m^{-2} (Fig. 4b). For example, the Nomex nanofibrous membrane with an areal density of 4.618 g m^{-2} still has $\eta = 99.76\%$ at a high-speed airflow of 15.83 cm s^{-1}. The test results indicate that Nomex nanofibrous membranes are able to capture $PM_{0.3}$ with high efficiency regardless of the airflow speed. It reflects the strong capture ability of the Nomex nanofibrous membrane and that Nomex nanofibrous membrane can still maintain an excellent physical structure under high shear stress brought by high-speed airflow.

The pressure drop of the Nomex nanofibrous membranes increases approximately linearly with the increase of area density and airflow velocity (Fig. 4c, d). For example, the pressure drop of the Nomex nanofibrous membrane with an areal density of 4.618 g m^{-2} increases significantly from 152.88 to 638.63 Pa as the airflow velocity increases from 4.17 to 15.83 cm s^{-1}. The results show that the directly proportional relationship between the airflow velocity and the pressure drop satisfies Darcy's law [65]. It means that the airflow is in the form of laminar flow through the porous Nomex nanofibrous membrane. Moreover, the QF is not significantly affected by the areal density at a constant airflow velocity (Fig. 4e), meaning that Nomex nanofibrous membranes with different areal densities all have excellent filtration quality. For example, the QF of the Nomex nanofibrous membrane decreases from 0.043 to 0.038 Pa^{-1} as the areal density increases from 1.553 to 4.618 g m^{-2} at an airflow rate of 5.33 cm s^{-1}. However, the QF values of the Nomex nanofibrous membranes decrease significantly with the airflow rate (Fig. 4f). Compared with a commercial glass fibrous filter commonly used for high-temperature filtration (areal density of 80.542 g m^{-2}, $\eta = 99.89\%$, $\Delta P = 264.60$ Pa, and $QF = 0.026$ Pa^{-1}), the Nomex nanofibrous membrane with an ultra-low areal density of 4.618 g m^{-2} exhibits a higher filtration efficiency for $PM_{0.3}$ ($\eta = 99.92\%$) with a lower pressure drop ($\Delta P = 189.47$ Pa) and a higher QF value ($QF = 0.038$ Pa^{-1}) at an airflow rate of 5.33 cm s^{-1} (Table S4). The above advantages can be attributed to the two following points: (1) the outstanding physical structure and strong polarity improve the PM capturing efficiency; (2) the strong slip effect reduces air resistance.

Efficient Filtering Mechanism

In the actual filtration process, the PM capture mechanisms through nanofibers can be classified into the following five

categories: direct interception, Brownian diffusion, inertia impact, gravity settling, and electrostatic deposition [66]. The filtration efficiency contributed by the first four capture mechanisms depends on fiber diameter, particle size, and airflow velocity. The first four mechanisms could be collectively referred to as intrinsic mechanisms [13, 24, 43]. Regarding the electrostatic deposition mechanism, many studies have shown that several polar functional groups are enriched on the PM surface, such as C–O, C=O, and C–N groups [24, 53]. When the polymer repeating unit has a stronger dipole moment, the polymer fiber behaves with stronger dipole–dipole and dipole-induced intermolecular forces, improving capture efficiency and capture stability for PM [67, 68]. The dipole–dipole and dipole-induced intermolecular forces between polar molecules are actually an electrostatic attraction between intrinsic dipole moments, we refer to this mechanism of electrostatic attraction to PMs as an intrinsic electrostatic deposition mechanism. The dipole moments of repeating units of Nomex, PTFE, PAN, and PP membranes were calculated through DFT. The calculation results show that the dipole moment of the repeating unit of Nomex reaches 4.87 D, which is greater than those of PTFE (0 D), PAN (4.05 D), and PP (0.43 D) (Fig. 4g). Therefore, the Nomex nanofibrous membranes are characterized by a more significant contribution of the intrinsic electrostatic deposition mechanism to capturing PM. Secondly, when the fibers are sufficiently thin, the occurrence of the slip effect will reduce the air resistance [69]. According to the air filtration theory, the dimensionless Knudsen number (Kn) is often used to characterize the flow state of the gas around the fiber, which is affected by the mean free path of air molecules (λ) and the average fiber diameter (d). Kn is written as:

$$\mathrm{Kn} = 2\lambda/d. \tag{3}$$

When $0.25 < \mathrm{Kn} < 10$, the airflow state belongs to the transition flow regime between the slip and free molecular flow [25]. The average diameter of the Nomex nanofibers is 111 nm, and the corresponding Kn value is 1.19; thus, the airflow state on the fiber surface belongs to the transition flow regime. In this case, the airflow is dominated by the large slip, and the mass transfer is dominated by the strong molecular diffusion [70], which means that gas molecules will be subjected to a strong slip flow effect as they move with the airflow over the fiber surface [71]. The slip flow effect reduces the resistance caused by the interaction between gas molecules and the fiber surface. Therefore, even if the average diameter of the Nomex nanofibers is greater than the mean free path of air molecules, it will not increase the airflow resistance. Due to the slip flow, Nomex nanofibrous membranes with a high Kn value can achieve a high-efficiency filtration with a low-pressure drop, thus possessing a high QF value. To demonstrate the filtration performance of the Nomex nanofibrous membrane for $PM_{0.3}$, the membrane with $QF = 0.043\ Pa^{-1}$ was continuously tested for 10 min with a tested airflow rate of 5.33 cm s^{-1}. The SEM images demonstrate that the Nomex nanofibers can capture a large quantity of the $PM_{0.3}$ NaCl aerosol (Fig. 4h, i), and the capturing mechanism is illustrated via the elemental mapping images obtained through SEM–EDS (Fig. S21a–d). The results demonstrate that the Nomex nanofibrous membrane with an average fiber diameter of 94 nm and an areal density of 4.618 g m^{-2} successfully captures a large amount of $PM_{0.3}$ (Fig. S21e–f). In addition, Nomex nanofibrous membrane has an excellent dust-holding capacity. The membrane with an areal density of 1.720 g m^{-2} can capture 6.046 g $PM_{0.3}$ per square meter, which is more than three times its own weight per unit area (Fig. S21g–h). A more intuitive demonstration is that the Nomex nanofibrous membrane can completely block smoke diffusion to the adjacent bottles (Fig. S22).

To explore the stability of the capturing efficiency of the membranes contributed by the intrinsic electrostatic deposition mechanism, the Nomex nanofibrous membranes were fumigated in isopropanol (IPA) for 24 h according to the ISO 16890 standard to remove static electricity [72]. The test result shows that the filtration efficiency of the Nomex nanofibrous membrane did not decrease significantly after IPA fumigation for 24 h (Fig. 4j). The filtration efficiency of the Nomex nanofibrous membrane with an areal density of 4.312 g m^{-2} for $PM_{0.3}$ only decreased from 99.79 to 99.60% after fumigation, which means that the filtration efficiency of the membrane for $PM_{0.3}$ is highly stable. A Nomex nanofibrous membrane with an areal density of 3.022 g m^{-2} was also soaked in deionized water for 24 h. After washing, its filtration efficiency for $PM_{0.3}$ remained at around 99% (Fig. S23). Therefore, it can be expected that the Nomex nanofibrous membranes have a high filtration efficiency even in humid environments or after being washed with water. The above experiments demonstrate that Nomex nanofibers have intrinsic high molecular dipole moments. In other words, Nomex nanofibers can have high filtration efficiency even when external charges are eliminated. To corroborate the long-term efficiency stability of the Nomex nanofibrous membranes for $PM_{0.3}$, the filtration efficiency of two membranes with areal densities of 1.929 and 4.618 g m^{-2} was tested for 15 consecutive days. The test results show that the filtration efficiency of the Nomex nanofibrous membrane with an areal density of 1.929 g m^{-2} fluctuates between 96 and 98% over the 15 days, while the filtration efficiency of the Nomex nanofibrous membrane with an areal density of 4.618 g m^{-2} decreases only from 99.92 to 99.87% (Fig. 4k).

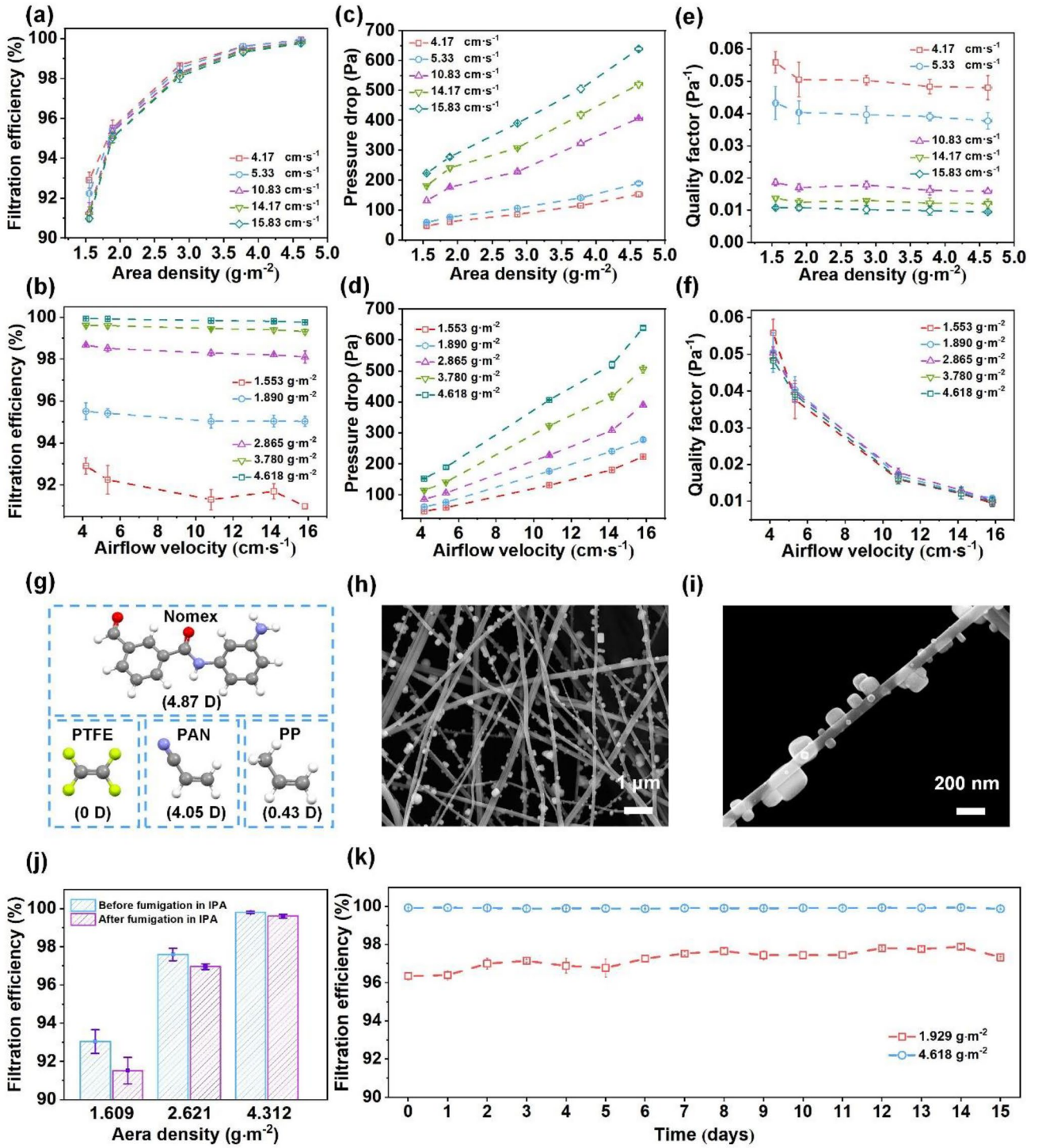

Fig. 4 Filtration performance of the Nomex nanofibrous membranes at room temperature. **a, b** Dependence of the filtration efficiency of the Nomex nanofibrous membranes with different areal densities on the airflow velocity. **c, d** Dependence of the pressure drop of the Nomex nanofibrous membranes with different areal densities on the airflow velocity. **e, f** Dependence of the *QF* values of the Nomex nanofibrous membranes with different areal densities on the airflow velocity. **g** Molecular model of the Nomex, PTFE, PAN, and PP filters and corresponding calculated dipole moments. **h, i** SEM images of the NaCl aerosols with $PM_{0.3}$ size captured by the Nomex nanofibers. **j** Comparison of the filtration efficiency before and after isopropyl alcohol fumigation for 24 h. **k** Results of the long-term filtration efficiency stability test of the Nomex nanofibrous membranes

Practical High-Temperature Filtration

To test the high-temperature filtration performance of the Nomex nanofibrous membranes, we built a high-temperature filtration device to simulate practical high-temperature filtration scenarios. The schematic diagram of the device is shown in Fig. 5a, and the details of its working mechanism can be found in the Experimental Section. We generated a large amount of PM by burning incense, which releases various air pollutants, including CO, SO_2, NO_2, and volatile organic compounds (VOCs). This approach is commonly used to simulate actual PM generation sources [53, 73]. Next, we tested the filtration efficiency of the Nomex nanofibrous membranes for $PM_{0.3–10}$ at a high temperature of 250 °C and airflow velocity of 5.33 cm s^{-1} using the high-temperature filtration device. The test results show that the Nomex nanofibrous membrane with an areal density of 4.631 g m^{-2} has a relatively high filtration efficiency (greater than 99.50%) for $PM_{0.3–10}$, meeting the required standard of high-efficiency filters (Fig. 5b). Figures 5c and S24 show the SEM images of the windward and leeward sides of the Nomex nanofibrous membrane after filtration at 250 °C for 10 min, respectively. The results show that the membrane successfully captured almost all PM at high temperature.

To investigate the dimensional stability of the Nomex nanofibrous membranes, in high temperatures, Nomex nanofibers, were observed by SEM, in a specific position, after heating at 150 °C, 200 °C, 250 °C, and 300 °C for 12 h (Fig. 5d). The SEM images show that the Nomex nanofibers retain their original microscopic morphology and position after long-term heating at 250 °C. We also placed the Nomex nanofibrous membranes in a muffle furnace for long-term heating. Commercial PTFE membranes, PAN, and PP nanofibrous membranes were also placed in the muffle furnace for comparison (Fig. 5e). After being heated at 150 °C, 200 °C, and 250 °C for 12 h, the Nomex nanofibrous membranes did not substantially shrink in size. However, the commercial PTFE membranes were severely deformed after being treated at 250 °C. As the heating temperature increased to 250 °C, the PAN nanofibrous filter shrank significantly and turned black. The PP nanofibrous membranes were severely deformed after treatment at only 150 °C and even melted at 200 °C (Fig. S25). These phenomena demonstrate the advantages of the Nomex nanofibrous membranes in terms of high-temperature dimensional stability.

To investigate the advantages of the Nomex nanofibrous membranes in high-temperature filtration, we compared their high-temperature filtration performance with that of other ordinary filters, such as PAN nanofibrous membranes and commercial filters (PP and PTFE) (Fig. 5f). To obtain these results, the following procedure was carried out: we placed these filters (size 25 cm (length) × 20 cm (width)) in a muffle furnace and heated them at a temperature ranging from 40 to 300 °C for 12 h, and then tested their filtration performance for $PM_{0.3}$. At an airflow velocity of 5.33 cm s^{-1}, as the temperature increased from 40 to 260 °C, the filtration efficiency of the Nomex nanofibrous membrane with an areal density of 4.618 g m^{-2} for $PM_{0.3}$ remained stable between 99.93 and 99.95%, which indicates the better filtration stability of this membrane compared with those of the commercial filters. Figure 5g shows the filtration efficiency of the Nomex nanofibrous membranes for $PM_{0.3}$ after being heated in a temperature range of 180–280 °C for 12 h. Even after being heated for 12 h at 280 °C, the Nomex nanofibrous membranes retain a filtration efficiency for $PM_{0.3}$ of 99.363%. We also used a Nomex nanofibrous membrane with an areal density of 4.212 g m^{-2} to filter vehicle exhausts (~ 70 °C) [13, 51]. The exhaust gas disappeared upon installing the Nomex nanofibrous filter, and the vehicle could normally run (Fig. 5h, Video S4). When the operating speed of the vehicle engine is 3000 rpm, the Nomex nanofibrous membrane could capture more than 97% of $PM_{0.3–10}$ emitted from the vehicle exhausts (Fig. S26).

To confirm that the filtration efficiency of the Nomex nanofibrous membranes for $PM_{0.3}$ remains stable for a long time at high temperature, we heated two Nomex nanofibrous membranes with areal densities of 2.525 and 4.631 g m^{-2} in the muffle furnace at 250 °C for 15 days. The filtration efficiency of these Nomex nanofibrous membranes for $PM_{0.3}$ over the 15–day period was tested using the TSI 8130A tester. Because of its ultra-fine diameter of ~ 100 nm and high intrinsic dipole moment of 4.87 D, the Nomex nanofibrous membrane has sustained high filtration efficiency and low air resistance after high-temperature treatment (Fig. 5i). For example, when a Nomex nanofibrous membrane with an areal density of 4.631 g m^{-2} was heated at 250 °C for 15 days, the $PM_{0.3}$ filtration efficiency was consistent between 99.92 and 99.94%. Overall, the Nomex nanofibrous membrane exhibits an array of excellent behaviors that are highly desirable for practical air filtration but generally difficult to achieve. Figure 5j compares the filtration efficiency, air resistance, cost, areal density, and working temperature of the Nomex nanofiber membrane with those of commercial PTFE filters, commercial ceramic nanofibrous filters, commercial PP filters, and reported PI fibrous membranes. Although the working temperature and air resistance perform slightly worse than PI nanofibrous membranes [51], other indexes are much superior to commercial PTFE, ceramic, and PP filters and PI fibrous membranes (Fig. 5j). It is worth noting that the Nomex nanofibrous membrane used at high temperature and room temperature can be washed with water or alcohol and reused for filtration applications, and can also be redissolved by the LiCl/DMAc solution system, reflecting the recyclability and renewability of the membrane (Fig. S27). The Nomex nanofibrous membrane exhibits the unprecedented integration of high filtration efficiency, high working temperature, low areal density, low air resistance, and

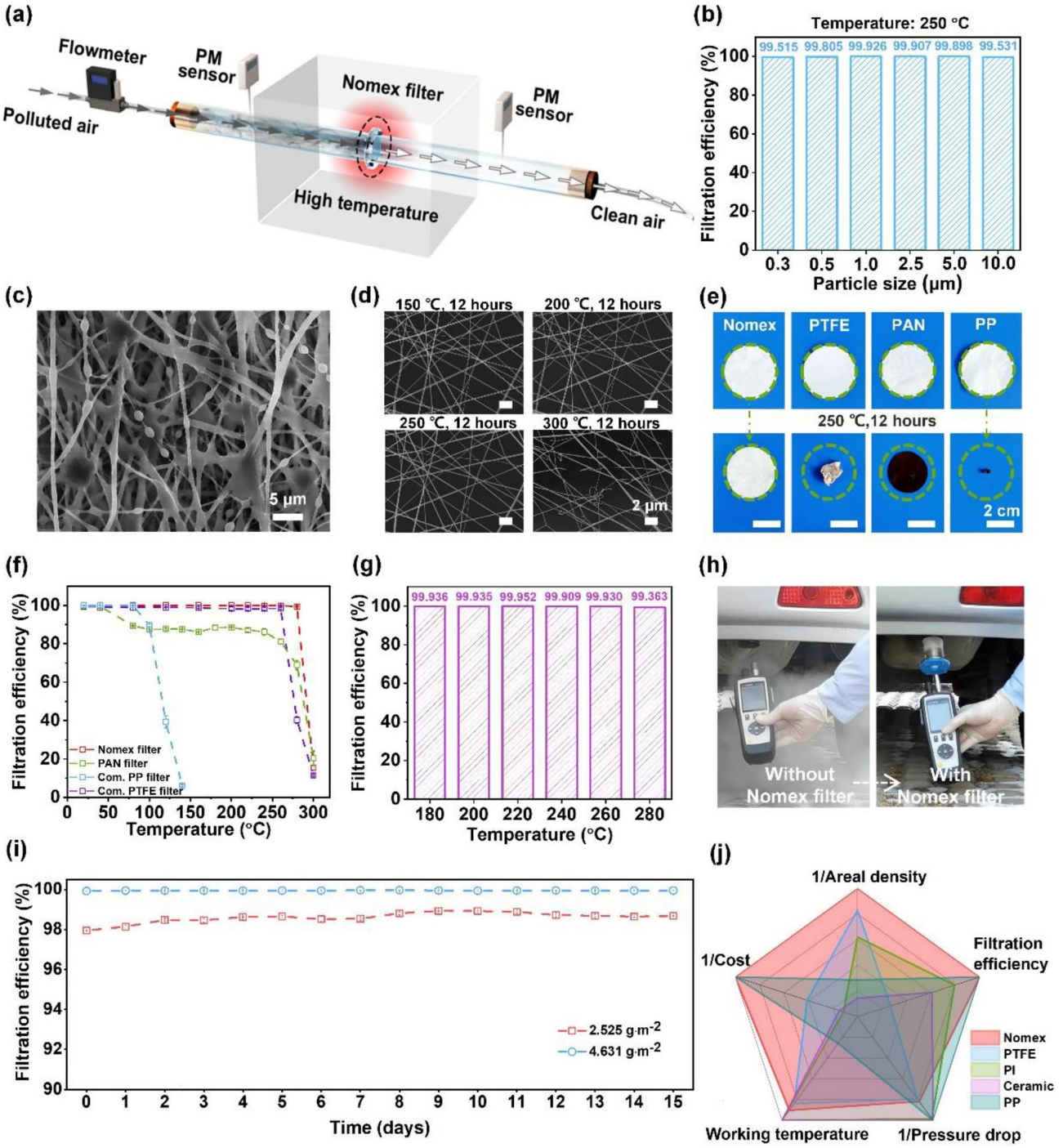

Fig. 5 Filtration performance of the Nomex nanofibrous membranes at high temperature. **a** Schematic diagram of the high-temperature filtration test device. **b** Filtration efficiency of the Nomex nanofibrous membranes for $PM_{0.3–10}$ at 250 °C via high-temperature filtration test device. **c** SEM image of the windward side of a Nomex nanofibrous membrane after polluted air filtration for 10 min at 250 °C. **d** SEM images of the Nomex nanofibrous membranes after heating at 150 °C, 200 °C, 250 °C, and 300 °C for 12 h. **e** Thermal shrinkage test images of the Nomex, PTFE, PAN, and PP membranes after heating at 250 °C for 12 h. **f** $PM_{0.3}$ removal efficiency of air filters made of different materials in the temperature range of 40–300 °C, "Com." stands for commercial. **g** Filtration efficiency of the Nomex nanofibrous membrane with an areal density of 4.618 g m^{-2} for $PM_{0.3}$ at 180–280 °C. **h** Images of the field filtration test for vehicle exhausts. **i** The filtration stability test results after long-term heating of the Nomex nanofibrous filter at 250 °C. **j** Radar chart of fibrous membrane comparing areal density, filtration efficiency, pressure drop, working temperature, and cost of Nomex nanofibrous membranes, commercial PTFE membranes, commercial ceramic nanofibrous membranes, commercial PP membranes, and PI nanofibrous membranes

low cost, combing with inherently excellent flame retardancy, chemical inertness, and mechanical properties, making them highly attractive for next generation advanced air filters.

Conclusions

In summary, we successfully developed hard-to-dissolve Nomex nanofibrous filters using a cost-effective and scalable ionic SBS method. The hard-to-dissolve Nomex microfibers were successfully dissolved into the precursor solution of the LiCl/DMAc system, and Nomex nanofibers with a diameter of about 100 nm were readily and stably prepared. The Nomex nanofibrous membrane with an areal density of only 4.618 g m^{-2} can filter up to 99.92% of NaCl aerosols with a diameter of 0.3 μm and with $\Delta P = 189.47$ Pa. The membrane can retain $\eta = 99.36\%$ for $PM_{0.3}$ after being heated at 280 °C for 12 h. Owing to their ultra-low weight, low cost, excellent high-temperature resistance, flame retardancy, acid corrosion resistance, stable filtration efficiency, and outstanding mechanical properties, Nomex nanofibrous membranes can be used in various fields that require PM-free air, such as precision electronics manufacturing, hospitals, and the aerospace industry. Most importantly, Nomex nanofibrous material is promising for high-temperature gas filtration in several industrial-grade fields, such as gas boilers, coal furnaces, glass factories, vehicle exhausts, and the chemical industry.

Supplementary Information The online version contains supplementary material available at https://doi.org/10.1007/s42765-022-00231-x.

Acknowledgements We appropriate the financial support of the Basic Science Center Program of the National Natural Science Foundation of China (NSFC) under Grant no. 51788104 and Beijing Natural Science Foundation under Grant no. JQ19005, and China Postdoctoral Science Foundation Grant no. 2021M691713.

Author contributions CJ, LL, and HW conceived the idea and supervised the research. ZKC, HYW, and LL designed the experiments. ZKC, CJ, and LL designed and constructed the experimental system. ZKC, CJ, ZWL, CY, BPZ, YQZ, YXW, LL, and HW synthesized the specimens and analyzed different characterizations. ZKC, HYW, CJ, LL, and HW contributed to writing the manuscript.

Declarations

Conflict of interest The authors declare that they have no conflict of interest.

References

1. Liao X, Dulle M, Silva JMDSE, Wehrspohn RB, Agarwal S, Förster S, Hou H, Smith P, Greiner A. High strength in combination with high toughness in robust and sustainable polymeric materials. *Science* **2019**;*366*:1376.
2. Vollrath F, Knight DP. Liquid crystalline spinning of spider silk. *Nature* **2001**;*410*:541.
3. Li L, Jia C, Liu Y, Fang B, Zhu W, Li X, Schaefer LA, Li Z, Zhang F, Feng X, Hussain N, Xi X, Wang D, Lin YH, Wei X, Wu H. Nanograin–glass dual-phasic, elasto-flexible, fatigue-tolerant, and heat-insulating ceramic sponges at large scales. *Mater Today* **2022**;*54*:72.
4. Li Z, Cui Z, Zhao L, Hussain N, Zhao Y, Yang C, Jiang X, Li L, Song J, Zhang B, Cheng Z, Wu H. High-throughput production of kilogram-scale nanofibers by Kármán vortex solution blow spinning. *Sci Adv* **2022**;*8*:eabn3690.
5. Shealy O. Development of new fibre and sheet structures-nomex nylon and spun-bonded products. *Textile Inst Ind* **1971**;*9*:10.
6. Tan J, Luo Y, Zhang M, Yang B, Li F, Ruan S. Dissolving and regeneration of meta-aramid paper: Converting loose structure into consolidated networks with enhanced mechanical and insulation properties. *ACS Appl Mater Interfaces* **2021**;*13*:16895.
7. Guan QF, Han ZM, Yang HB, Yang KP, Ling ZC, Yin CH, Zhao Y-X, Wang J-L, Yan B-B, Ma T, Hu B-C, Li C, Pan X-F, Chen S-M, Ma S-Y, Yu S-H. Biomimetic design and mass production of sustainable multiscale cellulose fibers-based hierarchical filter materials for protective clothing. *Adv Mater Technol* **2021**;*6*:2100193.
8. Huang T, Zhu Y, Zhu J, Yu H, Zhang Q, Zhu M. Self-reinforcement of light, temperature-resistant silica nanofibrous aerogels with tunable mechanical properties. *Adv Fiber Mater* **2020**;*2*:338.
9. Han Z, Wang J, Liu S, Zhang Q, Liu Y, Tan Y, Luo S, Guo F, Ma J, Li P, Ming X, Gao C, Xu Z. Electrospinning of neat graphene nanofibers. *Adv Fiber Mater* **2022**;*4*:268.
10. Zhang R, Liu C, Hsu PC, Zhang C, Liu N, Zhang J, Lee HR, Lu Y, Qiu Y, Chu S, Cui Y. Nanofiber air filters with high-temperature stability for efficient $PM_{2.5}$ removal from the pollution sources. *Nano Lett* **2016**;*16*:3642.
11. Brückner S, Liu S, Miró L, Radspieler M, Cabeza LF, Lävemann E. Industrial waste heat recovery technologies: an economic analysis of heat transformation technologies. *Appl Energy* **2015**;*151*:157.
12. Heidenreich S. Hot gas filtration—a review. *Fuel* **2013**;*104*:83.
13. Liu K, Liu C, Hsu P-C, Xu J, Kong B, Wu T, Zhang R, Zhou G, Huang W, Sun J, Cui Y. Core–shell nanofibrous materials with high particulate matter removal efficiencies and thermally triggered flame retardant properties. *ACS Cent Sci* **2018**;*4*:894.
14. Liu H, Zhang S, Liu L, Yu J, Ding B. High-performance $PM_{0.3}$ air filters using self-polarized electret nanofiber/nets. *Adv Funct Mater* **2020**;*30*:1909554.
15. Huang Z, Dang C, Sun Z, Qi H. High-efficiency air filter media with a three-dimensional network composed of core–shell zeolitic imidazolate Framework-8@Tunicate nanocellulose for $PM_{0.3}$ removal. *ACS Appl Mater Interfaces* **2021**;*13*:57921.
16. Badran G, Verdin A, Grare C, Abbas I, Achour D, Ledoux F, Roumie M, Cazier F, Courcot D, Lo Guidice J-M, Garçon G. Toxicological appraisal of the chemical fractions of ambient fine ($PM_{2.5–0.3}$) and quasi-ultrafine ($PM_{0.3}$) particles in human bronchial epithelial BEAS-2B cells. Environ Pollut. 2020;263:114620.
17. Editoral. Clean air for a sustainable world. Nat Commun. 2021;12:5824.
18. Wu X, Nethery RC, Sabath MB, Braun D, Dominici F. Air pollution and COVID-19 mortality in the United States: strengths and limitations of an ecological regression analysis. Sci Adv. 2020;6:eabd4049.
19. Magazzino C, Mele M, Schneider N. The relationship between air pollution and COVID-19-related deaths: an application to three French cities. *Appl Energy* **2020**;*279*:115835.
20. Plail M. A conversation on the impacts and mitigation of air pollution. *Nat Commun* **2021**;*12*:5822.

21. Zhang R, Liu C, Zhou G, Sun J, Liu N, Hsu P-C, Wang H, Qiu Y, Zhao J, Wu T, Zhao W, Cui Y. Morphology and property investigation of primary particulate matter particles from different sources. *Nano Res* **2018**;*11*:3182.
22. Zhang S, Liu H, Tang N, Ali N, Yu J, Ding B. Highly efficient, transparent, and multifunctional air filters using self-assembled 2D nanoarchitectured fibrous networks. *ACS Nano* **2019**;*13*:13501.
23. Srikrishnarka P, Kumar V, Ahuja T, Subramanian V, Selvam AK, Bose P, Jenifer SK, Mahendranath A, Ganayee MA, Nagarajan R, Pradeep T. Enhanced capture of particulate matter by molecularly charged electrospun nanofibers. *ACS Sustain Chem Eng* **2020**;*8*:7762.
24. Liu C, Hsu P-C, Lee H-W, Ye M, Zheng G, Liu N, Li W, Cui Y. Transparent air filter for high-efficiency $PM_{2.5}$ capture. Nat Commun. 2015;6:6205.
25. Li P, Wang C, Zhang Y, Wei F. Air filtration in the free molecular flow regime: a review of high-efficiency particulate air filters based on carbon nanotubes. *Small* **2014**;*10*:4543.
26. Hu M, Wang Y, Yan Z, Zhao G, Zhao Y, Xia L, Cheng B, Di Y, Zhuang X. Hierarchical dual-nanonet of polymer nanofibers and supramolecular nanofibrils for air filtration with a high filtration efficiency, low air resistance and high moisture permeation. *J Mater Chem A* **2021**;*9*:14093.
27. Liu H, Zhang S, Liu L, Yu J, Ding B. High-performance filters from biomimetic wet-adhesive nanoarchitectured networks. *J Mater Chem A* **2020**;*8*:18955.
28. Zhang A, Li H, Zhang A, Zhou J, Yan Y. High-temperature bearable polysulfonamide/polyacrylonitrile composite nanofibers for high-efficiency $PM_{2.5}$ filtration. Compos Commun. 2021;23:100582.
29. Pan T, Liu J, Deng N, Li Z, Wang L, Xia Z, Fan J, Liu Y. ZnO Nanowires@PVDF nanofiber membrane with superhydrophobicity for enhanced anti-wetting and anti-scaling properties in membrane distillation. *J Membr Sci* **2021**;*621*:118877.
30. Lee HR, Liao L, Xiao W, Vailionis A, Ricco AJ, White R, Nishi Y, Chiu W, Chu S, Cui Y. Three-dimensional analysis of particle distribution on filter layers inside N95 respirators by deep learning. *Nano Lett* **2021**;*21*:651.
31. Liang H-W, Wang L, Chen P-Y, Lin H-T, Chen L-F, He D, Yu S-H. Carbonaceous nanofiber membranes for selective filtration and separation of nanoparticles. *Adv Mater* **2010**;*22*:4691.
32. Wang H, Lin S, Yang S, Yang X, Song J, Wang D, Wang H, Liu Z, Li B, Fang M, Wang N, Wu H. High-temperature particulate matter filtration with resilient yttria-stabilized ZrO_2 nanofiber sponge. *Small* **2018**;*14*:1800258.
33. Liebermann F. Dynamic cross flow filtration with Novoflow's single shaft disk filters. *Desalination* **2010**;*250*:1087.
34. Zhang C, Jiang Y-X, Sun J-P, Xiao H, Shi M-W, Long J-J. Investigation of the influence of supercritical carbon dioxide treatment on meta-aramid fiber: thermal decomposition behavior and kinetics. J CO_2 Util. 2020;37:85.
35. Panar M, Beste LF. Structure of poly(1,4-benzamide) solutions. *Macromolecules* **1977**;*10*:1401.
36. Shogbon CB, Brousseau JL, Zhang H, Benicewicz BC, Akpalu YA. Determination of the molecular parameters and studies of the chain conformation of polybenzimidazole in DMAc/LiCl. *Macromolecules* **2006**;*39*:9409.
37. Wang B, Tang Y, Wen Z, Wang H. Dissolution and regeneration of polybenzimidazoles using ionic liquids. *Eur Polym J* **2009**;*45*:2962.
38. Byun S, Lee SH, Song D, Ryou M-H, Lee YM, Park WH. A crosslinked nonwoven separator based on an organosoluble polyimide for high-performance lithium-ion batteries. *J Ind Eng Chem* **2019**;*72*:390.
39. Wang ZY, Fu ZJ, Shao DD, Lu MJ, Xia QC, Xiao HF, Su BW, Sun SP. Bridging the miscibility gap to fabricate delamination-free dual-layer nanofiltration membranes via incorporating fluoro substituted aromatic amine. *J Membr Sci* **2020**;*610*:118270.
40. Sayyed AJ, Deshmukh NA, Pinjari DV. A critical review of manufacturing processes used in regenerated cellulosic fibres: Viscose, cellulose acetate, cuprammonium, LiCl/DMAc, ionic liquids, and NMMO based lyocell. *Cellulose* **2019**;*26*:2913.
41. Duchemin B-C. Structure, property and processing relationships of all-cellulose composites: University of Canterbury. 2008.
42. Jia C, Li L, Song J, Li Z, Wu H. Mass production of ultrafine fibers by a versatile solution blow spinning method. *Acc Chem Res* **2021**;*2*:432.
43. Khalid B, Bai X, Wei H, Huang Y, Wu H, Cui Y. Direct blow-spinning of nanofibers on a window screen for highly efficient $PM_{2.5}$ removal. Nano Lett. 2017;17:1140.
44. Frisch M, Trucks G, Schlegel H. Gaussian 09. Revision D. 01 [CP]. Pittsburgh USA: Gaussian. Inc., Wallingford CT. 2013.
45. Sannigrahi A, Arunbabu D, Sankar RM, Jana T. Aggregation behavior of polybenzimidazole in aprotic polar solvent. *Macromolecules* **2007**;*40*:2844.
46. Yan J, Dong K, Zhang Y, Wang X, Aboalhassan AA, Yu J, Ding B. Multifunctional flexible membranes from sponge-like porous carbon nanofibers with high conductivity. *Nat Commun* **2019**;*10*:5584.
47. Fu Q, Duan C, Yan Z, Li Y, Si Y, Liu L, Yu J, Ding B. Nanofiber-based hydrogels: controllable synthesis and multifunctional applications. *Macromol Rapid Commun* **2018**;*39*:1800058.
48. Huang Y, Song J, Yang C, Long Y, Wu H. Scalable manufacturing and applications of nanofibers. *Mater Today* **2019**;*28*:98.
49. Guan Q-F, Han Z-M, Ling Z-C, Yang H-B, Yu S-H. Sustainable wood-based hierarchical solar steam generator: A biomimetic design with reduced vaporization enthalpy of water. *Nano Lett* **2020**;*20*:5699.
50. Sun Y, Mwandeje JB, Wangatia LM, Zabihi F, Nedeljković J, Yang S. Enhanced photocatalytic performance of surface-modified TiO_2 nanofibers with rhodizonic acid. *Adv Fiber Mater* **2020**;*2*:118.
51. Li Z, Song J, Long Y, Jia C, Liu Z, Li L, Yang C, Liu J, Lin S, Wang H, Liu Y, Fang M, Wu H. Large-scale blow spinning of heat-resistant nanofibrous air filters. *Nano Res* **2020**;*13*:861.
52. Dong Y, Zheng Y, Zhang K, Yao Y, Wang L, Li X, Yu J, Ding B. Electrospun nanofibrous materials for wound healing. *Adv Fiber Mater* **2020**;*2*:212.
53. Kim J, Chan Hong S, Bae GN, Jung JH. Electrospun magnetic nanoparticle-decorated nanofiber filter and its applications to high-efficiency air filtration. *Environ Sci Technol* **2017**;*51*:11967.
54. Xu W, Hu X, Zhuang S, Wang Y, Li X, Zhou L, Zhu S, Zhu J. Flexible and salt resistant janus absorbers by electrospinning for stable and efficient solar desalination. *Adv Energy Mater* **2018**;*8*:1702884.
55. Moon J, Bui TT, Jang S, Ji S, Park JT, Kim M-G. A highly efficient nanofibrous air filter membrane fabricated using electrospun amphiphilic PVDF-g-POEM double comb copolymer. *Sep Purif Rev* **2021**;*279*:119625.
56. Zhang X, Liu J, Zhang H, Hou J, Wang Y, Deng C, Huang C, Jin X. Multi-layered, corona charged melt blown nonwovens as high performance $PM_{0.3}$ air filters. *Polymers* **2021**;*13*:485.
57. Wang N, Raza A, Si Y, Yu J, Sun G, Ding B. Tortuously structured polyvinyl chloride/polyurethane fibrous membranes for high-efficiency fine particulate filtration. *J Colloid Interface Sci* **2013**;*398*:240.
58. Wang N, Zhu Z, Sheng J, Al-Deyab SS, Yu J, Ding B. Superamphiphobic nanofibrous membranes for effective filtration of fine particles. *J Colloid Interface Sci* **2014**;*428*:41.
59. Jiang Z, Zhang H, Zhu M, Lv D, Yao J, Xiong R, Huang C. Electrospun soy-protein-based nanofibrous membranes for effective antimicrobial air filtration. *J Appl Polym Sci* **2018**;*135*:45766.

60. Wang Y, Li W, Xia Y, Jiao X, Chen D. Electrospun flexible self-standing γ-alumina fibrous membranes and their potential as high-efficiency fine particulate filtration media. *J Mater Chem A* **2014**;*2*:15124.
61. Xu W, Fu W, Meng X, Tang M, Huang C, Sun Y, Dai Y. One stone two birds: a sinter-resistant TiO_2 nanofiber-based unbroken mat enables PM capture and in situ elimination. *Nanoscale* **2021**;*13*:20564.
62. Chen X, Wang W, Li S, Jiao C. Fire safety improvement of para-aramid fiber in thermoplastic polyurethane elastomer. *J Hazard Mater* **2017**;*324*:789.
63. Su L, Niu M, Lu D, Cai Z, Li M, Wang H. A review on the emerging resilient and multifunctional ceramic aerogels. *J Mater Sci Technol* **2021**;*75*:1.
64. Zhang J, Gong S, Wang C, Jeong D-Y, Wang ZL, Ren K. Biodegradable electrospun poly(lactic acid) nanofibers for effective $PM_{2.5}$ removal. *Macromol Mater Eng* **2019**;*304*:1900259.
65. Whitaker S. Flow in porous media I: a theoretical derivation of Darcy's law. *Transp Porous Media* **1986**;*1*:3.
66. Chen CY. Filtration of aerosols by fibrous media. *Chem Rev* **1955**;*55*:595.
67. Lee S, Cho AR, Park D, Kim JK, Han KS, Yoon I-J, Lee MH, Nah J. Reusable polybenzimidazole nanofiber membrane filter for highly breathable $PM_{2.5}$ dust proof mask. *ACS Appl Mater Interfaces* **2019**;*11*:2750.
68. Xu J, Liu C, Hsu P-C, Liu K, Zhang R, Liu Y, Cui Y. Roll-to-roll transfer of electrospun nanofiber film for high-efficiency transparent air filter. *Nano Lett* **2016**;*16*:1270.
69. Song J, Li Z, Wu H. Blowspinning: a new choice for nanofibers. *ACS Appl Mater Interfaces* **2020**;*12*:33447.
70. Hung C-H, Leung WW-F. Filtration of nano-aerosol using nanofiber filter under low Peclet number and transitional flow regime. Sep Purif Rev. 2011;79:34.
71. Zhang Z, Liu BYH. Experimental study of aerosol filtration in the transition flow regime. *Aerosol Sci Technol* **1992**;*16*:227.
72. International organization for standardization. ISO 16890: air filters for general ventilation. Switzerland. 2016.
73. Schoental R, GlBbard S. Carcinogens in chinese incense smoke. *Nature* **1967**;*216*:612.

Zekun Cheng is a Ph.D. student under the supervision of Prof. Hui Wu at the School of Materials Science and Engineering, Tsinghua University. His research interests mainly focus on developing novel methods for preparing nanofibers and the multifunctional applications of nanofibers.

Haiyang Wang received his B.S. degree from Northwestern Polytechnical University in 2015. He is currently pursuing his Ph.D. degree under the supervision of Prof. Zhen Xu at Tsinghua University, China. His research focuses on nanofibers.

Ziwei Li is a graduate student at Tsinghua University under the supervision of Prof. Hui Wu. His research interests focus on the fabrication and applications of nanofiber materials.

Chong Yang received his Ph. D. degree from Huazhong University of Science and Technology (P.R. China) in 2020. He is currently a postdoctoral fellow in the laboratory of Prof. Hui Wu at Tsinghua University. His research focuses on fabricating various nanofibers and their application in air filtration.

Baopu Zhang received his B.E. degree under the guidance of Prof. Hui Wu from Tsinghua University in 2022. His research focused on the preparation and application of nanofibers. He is going to pursue his Ph.D. degree at the Chemical Engineering Department of the Massachusetts Institute of Technology.

Yiqian Zhou received her B.E. degree from Tsinghua University in 2022. She is currently pursuing her Ph.D. degree under the supervision of Prof. Hui Wu at Tsinghua University, China. Her research focuses on high-temperature thermal insulation and brain-computer interface electrode.

Yuxuan Wang is currently pursuing his B.S. degree and B.Eng degree at Tsinghua University, China. His research focuses on the mass production and application of low-dimensional materials.

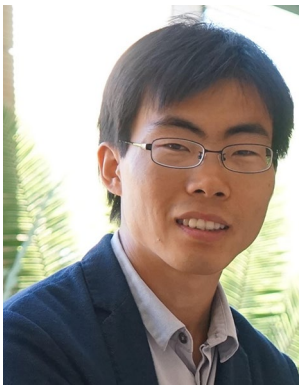

Chao Jia is an associate professor at the College of Materials Science and Engineering, Donghua University. He obtained his Ph.D. degree from the Beijing Institute of Technology in 2018. He worked as a postdoctoral research associate at Tsinghua University from 2018 to 2021. His research interests focus on nanofibers, cellulose nanomaterials, and wood-based functional materials.

Lei Li is an assistant professor at the School of Mechanical Engineering, Beijing Institute of Technology. He received his Ph.D. from the Beijing Institution of Technology in 2020. He worked as a postdoctoral research associate at School of Materials Science and Engineering, Tsinghua University from 2020 to 2022. His research interests include the battery safety, biodegradable polymer preparation, and ceramic nanofibers.

Hui Wu is an associate professor at the School of Materials Science and Engineering, Tsinghua University. He obtained his Ph.D. degree from Tsinghua University in 2009. He worked as a postdoctoral research associate at Stanford University from 2009 to 2013. His research interests focus on nanofibers, energy storage materials, and flexible electronics.